Modification of gum ghatti *via* grafting with acrylamide and analysis of its flocculation, adsorption, and biodegradation properties

Hemant Mittal[1*], Vaneet Kumar[2], Saeed M Alhassan[1] and Suprakas Sinha Ray[3,4*]

[1]Department of Chemical Engineering, Khalifa University of Science and Technology, PO Box 2533, Abu Dhabi, United Arab Emirates

[2]Department of Applied Science, CT Group of Institutions Shahpur, Jalandhar, Punjab, India

[3]DST/CSIR National Centre for Nanostructured Materials, Council for Scientific and Industrial Research, Pretoria 0001, South Africa

[4]Department of Applied Chemistry, University of Johannesburg, Doornfontein 2028, South Africa

*Corresponding authors.
E-mail addresses: mittal.hemant5@gmail.com (HM); rsuprakas@csir.co.za (SSR), suprakas73@yahoo.com (SSR)

Abstract

In this work, an environmentally friendly gum ghatti-crosslinked-polyacrylamide (Gg-cl-PAAM) hydrogel was synthesized from gum ghatti (Gg) and acrylamide (AAM) using a microwave-assisted grafting technique, and tested for use in water purification applications as an adsorbent and flocculent. The Gg-cl-PAAM was characterized using SEM, FTIR, and TGA, and displayed pH responsive swelling behavior, with maximum swelling (2117%) observed in solution with neutral pH. The flocculation characteristics of Gg-cl-PAAM were tested in clay solutions as a function of pH, temperature, and the polymer mass loading, showing that the best performance is obtained at neutral pH at 40 ºC. The adsorption capacities of Gg-cl-PAAM for the removal different dyes such as brilliant green (BG), rhodamine B (RhB), congo red (CR), and methyl orange (MO) were tested, revealing that the adsorption of all dyes followed the Langmuir isotherm model, with q_m values of 523.62 mg g^{-1} for BG, 421.60 mg g^{-1} for RhB, 179.09 mg g^{-1} for CR, and 173.69 mg g^{-1} for MO. Finally, the environmentally friendly nature of Gg-cl-PAAM was examined using the soil-burial composting method, which demonstrated 93% degradation of the Gg-cl-PAAM hydrogel within 60 days.

Keywords: Biodegradable hydrogel; flocculation; dye removal; adsorption

1. Introduction

The development of commercially viable "biodegradable green products" for both matrices and reinforcement materials based on gum polysaccharides is on the rise as a result of the non-degradable nature of certain synthetic polymers [1-4]. In contrast to such synthetic polymers, gum polysaccharides are biodegradable, cost-effective, and biocompatible; nevertheless, in their native form, they exhibit very poor mechanical and physical properties. Grafting is the most widely studied and used technique that can be used to improve the characteristics and properties of gum polysaccharides. The resultant graft co-polymers possess properties that are derived from both components—for example, they retain the environmentally friendly nature and low toxicity of gum polysaccharides, while adopting the enhanced mechanical properties associated with synthetic monomers [5-7].

Flocculation is a well-known process in wastewater treatment technology that involves the settlement of colloidal suspensions of particles of different impurities by converting them into heavier and larger flocs. Polyelectrolytes are critical in the flocculation process because of their ability to interact with the positively charged particles in aqueous colloidal dispersions. The flocculation behavior of a material is largely dependent on the physico-chemical property profiles of the flocculent and the medium [8-12]. Polymer-based flocculants have gathered significant of attention owing to their ability to destabilize colloidal particles and create bridges between them [9, 13-15]. Flocculants based on synthetic polymers generally display much better performance and require the use of comparatively smaller amounts in order to achieve the desired performance when compared to biopolymer-based flocculants [16, 17]. In spite of their excellent performance, the majority of flocculants based on synthetic polymers are non-

biodegradable and are more expensive than biopolymer-based flocculants. In order to overcome these challenges, polysaccharide-based biodegradable hydrogels were used in the past as flocculants to remove suspended particles from colloidal solutions [5-7, 11, 18, 19].

Applications involving dyes are quite diverse and most of them are associated with adverse effects on human health [20]. Therefore, proper treatment of extremely dangerous and harmful dyes containing industrial effluents is critical prior to their discharge into different water bodies. Gum polysaccharide-based hydrogels have been used previously in water purification applications, however, most of the hydrogels were found to be either resistant to biodegradation or possessed very poor property profiles [21, 22]. In a study by Yadav *et al.* [23] κ-carrageenan-based non-biodegradable material was utilized as a flocculent for the removal of coking coals [23]. Alginate and 2-acrylamidoglycolic acid based non-biodegradable hydrogels were also used as flocculent and adsorbent [24]. Previously, we have also utilized gum polysaccharide-based hydrogels as adsorbents and flocculants [6, 7, 11, 19]. However, the preparation of hydrogels using conventional grafting techniques typically involves long reaction times and the resulting materials often possess low swelling capacity. These limitations can be overcome by utilizing microwave irradiation for the generation of free radicals, which shortens the reaction time significantly and ensures the formation of short chain polymers [25]. In the past, hydrogels synthesized via microwave-assisted methods have shown improved swelling characteristics when compared to hydrogels synthesized in-air or under pressure [26]. Therefore, in the present work, we use microwave-assisted grafting to synthesize a biodegradable hydrogel from gum ghatti (Gg) and acrylamide (AAM), and utilize this hydrogel as a flocculent and adsorbent in water purification applications. In addition, the biodegradability of the hydrogel is tested via the soil burial composting technique, and the progression of the degradation process is monitored by

examining the changes in the morphological and structural characteristics of the hydrogel samples.

2. Experimental

2.1. Materials

AAM (purity ≥ 99 %), Gg (purity ≥95 %), ascorbic acid (ABC) (reagent grade), potassium persulfate (KPS) (ACS reagent, purity ≥95 %), *N*,*N'*-methylene-bis-acrylamide (MBA) (purity ≥ 99 %), brilliant green (BG) (dye content 90 %), rhodamine B (RhB) (dye content 95 %), congo red (CR) (analytical grade), methyl orange (MO) (ACS reagent, dye content 85 %), and kaolin (anhydrous free flowing) were purchased from Sigma Aldrich (South Africa) and used as received.

2.2. Synthesis of hydrogel

A gum ghatti-crosslinked-polyacrylamide (Gg-cl-PAAM) hydrogel was synthesized via microwave-assisted grafting and the details of the optimization of different physical and chemical grafting parameters are given in Table 1. Briefly, fixed amounts of KPS and ABC were added to the dispersion of Gg (1.0 g) in double-distilled water (10 mL). Thereafter, specific amounts of MBA and AAM were added to the reaction mixture. The reactants were mixed thoroughly in a beaker, which was kept subsequently in a conventional domestic microwave (Samsung, India) for a set amount of time. The unreacted monomer, homopolymer, and copolymers were extracted with continuous washings with acetone. The resultant material was dried in a hot-air oven at 60 ºC and crushed to powder using ball mill. Different grafting parameters were calculated according to the expressions given in our previous publication [27] and reported in Table 1. The optimized physical and chemical reaction parameters based on the

values of percentage swelling (P_s) were determined as follows: reaction time = 90 s; volume of double-distilled water = 10 mL; initiator ratio (i.e., ABC:KPS) = 0.5:1; concentration of AAM = 0.9859 mol L^{-1}, and concentration of MBA = 0.0974 mol L^{-1} (Table 1).

2.3. Characterization

The introduction of different functional groups into the Gg after grafting and at different stages of degradation was studied using Fourier transform infrared (FTIR) spectroscopy (Perkin-Elmer Spectrum 100 spectrometer, USA) using the KBr pellet method in the spectral range 4000–400 cm^{-1} with a resolution of 4 cm^{-1} and 32 scans. The morphological changes in Gg after grafting and during degradation were studied using scanning electron microscopy (SEM) (JEOL- JSM 7500F Scanning Electron Microscope, Japan) under a 20-kV electron acceleration voltage. The samples of hydrogels were not conducting, and, therefore, carbon coating was added to render them conducting. The TGA and DTG thermograms of Gg and Gg-cl-PAAM were obtained using a TGA/DTA/DTG thermogravimetric analyzer (Perkin-Elmer TGA 4000, USA) under air atmosphere at a heating rate of 10 °C/min.

2.4. Swelling studies

The water absorption properties of Gg-cl-PAAM were examined with respect to different swelling parameters such as swelling time, temperature, and pH. Initially, a fixed amount of Gg-cl-PAAM was added to distilled water (100 mL) at neutral pH. The samples were allowed to swell and after a desired time interval (4, 8, 12, 16, 20, and 24 h), weight of the swelled samples were taken. The effects of varied solution temperature (30, 40, 50, 60, and 70 °C) and solution pH (from 3.0 to 13.0) on P_s were studied using the same swelling procedure.

2.5. Separation of saline from petroleum fractions

The ability of Gg-cl-PAAM hydrogel to absorb saline (1 wt% NaCl solution) from its emulsions with different petroleum fractions such as diesel, petrol, petroleum ether, and kerosene were tested. The petroleum fraction–saline emulsions of saline water (25 mL) with individual petroleum fraction (25 mL) were prepared and tween-20 (10 mL) was added to each emulsion as an emulsifier. Subsequently, 100 mg of Gg-cl-PAAM was added and each emulsion was shaken for 24 h at an agitation speed of 200 rpm. Once the agitation was stopped, the emulsions were allowed to separate by leaving the flasks undisturbed for 48 h. The petroleum fractions were separated to measure the amount of saline water absorbed by Gg-cl-PAAM.

2.6. Flocculation studies

The flocculation capacity of Gg-cl-PAAM was examined in a clay suspension (50 ppm kaolin solution) following the standard jar test [28]. The effects of different parameters such as polymer dose, temperature, and pH of the clay suspension on the flocculation capacity were evaluated. A specific amount of the polymer was added to 1000 mL of the kaolin solution and the mixture was stirred for 5 min at an agitation speed of 100 rpm, followed by a comparatively low stirring speed of 50 rpm for 2 min. The solution was kept undisturbed for 15 min to allow the flocs to settle. To measure the residual turbidity, 5 mL of the sample were taken from a depth of 3 cm once the flocs were settled. The effects of solution temperature and pH were studied at temperature ranging from 30 to 60 °C and at a pH of clay suspension of 4, 7, and 9.2.

2.7. Adsorption of synthetic dyes

The adsorption behavior of Gg-cl-PAAM was tested by examining its capacity to adsorb two cationic dyes, namely RhB and BG, and two anionic dyes, CR and MO. For each adsorption experiment, 50 mg L^{-1} (C_o) solution of one dye (50 mL) was agitated in a 100-mL glass bottle

containing a fixed mass of Gg-cl-PAAM. Once the agitation was stopped, the concentration of the dye left in the bulk solution (C_e) was determined by first filtering the dye solutions using a 0.45-μm PVDF syringe filter and subsequently by analyzing it by UV-Vis spectrophotometery (Perkin Elmer LAMBDA 750S, USA). The percentage removal was calculated using Eq. (1):

$$\%\, removal = \frac{(C_o - C_e)}{C_o} \times 100 \qquad (1)$$

The adsorption isotherms for all four dyes were studied at 25 ºC, with the dyes in 50 to 400 mg L^{-1} concentration range. In each case, a 50-mL dye solution at a specific concentration (C_o) was mixed with an optimized amount of adsorbent. After agitation, the solutions were filtered and the equilibrium adsorption capacity (q_e) was calculated using the following expression:

$$q_e = \frac{(C_o - C_e)}{m} \times V \qquad (2)$$

The ability of Gg-cl-PAAM to act as a reusable adsorbent was checked only for the RhB dye. Desorption studies were performed for five successive cycles. Initially, RhB dye molecules were adsorbed onto the hydrogel polymer particles, the adsorption efficiency was calculated, and the dye-loaded adsorbent particles were separated from the solution by vacuum filtration and dried in a hot-air oven. The dye-loaded dry particles of hydrogel polymer were added to 50 mL of acetone and agitated for 4 h. Subsequently, the particles were separated, dried, and used again in the next cycle. This process of adsorption and desorption was repeated for five consecutive cycles.

2.8. Biodegradation studies

Biodegradation is one of the most unique and important properties of biopolymers and it should be unaffected by the different modification processes. Therefore, the biodegradation behavior of

the Gg-cl-PAAM hydrogel was examined through the well-known and extensively studied soil-burial method. The detailed experimental procedure is reported in our previous work [7]. In brief, rectangular samples of Gg-cl-PAAM with particular dimensions and weight (W_i) were buried in the compost kept in a flower pot. In order to minimize water loss, water from a municipal sewerage plant was added to the compost every second day. Subsequently, one sample was taken out of the compost every 5 days, washed with distilled water, and weighed (W_t). The change in weight after every 5 days was calculated using Eq. (3) [7]:

$$\text{Decrease in weight (\%)} = \frac{W_i - W_t}{W_i} \times 100 \qquad (3)$$

3. Results and discussion

3.1. Synthesis of Gg-cl-PAAM

3.1.1. Mechanism of synthesis of Gg-cl-PAAM hydrogel

Initially, the initiators generate $SO_4^{\bullet-}$ radical anions and $OH^{\bullet}$ radicals that subsequently generate active sites on Gg and AAM molecules, starting the grafting reactions. The reaction is further propagated by the activated backbone and monomer molecules and results in the formation of crosslinked hydrogel polymer Gg-cl-PAAM (Figure 1).

3.1.2. Characterization

3.1.2.1. FTIR

The FTIR spectrum of grafted hydrogel exhibited peaks at 1669 cm^{-1}, corresponding to the C=O amide I stretching band, and at 1458 cm^{-1}, corresponding to the NH in plane bending of amide II band. In addition, peaks associated with the CN stretching vibrations of amide III band and the

OCN deformations of amide IV band were observed at 1109 cm^{-1} and 606 cm^{-1}, respectively, along with the peaks characteristic for Gg [26] (Figure 2). The presence of peaks associated with these functional groups in the FTIR spectrum of Gg-cl-PAAM suggested that AAM was grafted onto Gg successfully.

3.1.2.2. Thermal studies

TGA of Gg-cl-PAAM revealed several decomposition stages in the temperature range from 149.3 to 615.7 °C (Figure 3(a)). The first stage of thermal decomposition, associated with dehydration and initial depolymerization, was observed in the range from 149.3 to 341.7 °C, and accounted for a percentage weight loss of 34.1%. The decomposition caused by the progression of the depolymerization and initial breakdown of different polymeric chains occurred between 341.7 and 586.0 °C, and accounted for a 41.7% weight loss. The final decomposition stage, which corresponded to the complete breakdown of the polymer structure, was observed between 586.0 and 615.7 °C, and represented a weight loss of 18.2% (Figure 3(a)). The Gg-cl-PAAM exhibited lower initial decomposition temperature (IDT) and higher final decomposition temperature (FDT) than the pristine Gg [29]. The lower IDT of Gg-cl-PAAM as compared to Gg was due to the release of ammonia gas during the formation of imide groups in grafting reactions. However, after the formation of imide group, the thermal stability of the crosslinked graft co-polymer, i.e. Gg-cl-PAAM increased resulting in the higher FDT as compared to Gg [19]. Comparison of the percentage decomposition also revealed that although about 20% of the thermal decomposition occurred essentially within the same temperature range for Gg and Gg-cl-PAAM, the Gg-cl-PAAM hydrogel exhibited much better thermal stability than Gg as a result of the introduction of imide groups (Table 2).

The DTG of Gg-cl-PAAM (Figure 3(b)) exhibited peaks at 230.2 °C (mass-loss = 0.30 mg min^{-1}), 377.5 °C (mass-loss = 0.38 mg min^{-1}), and 594.5 °C (mass-loss = 0.873 mg min^{-1}). Comparison of the DTG of Gg-cl-PAAM with that of Gg showed that for Gg-cl-PAAM, the thermal degradation took place at comparatively higher temperature with significantly lower mass-loss when compared to Gg [29]. The Gg-cl-PAAM displayed T_{max} at 594.5 °C, whereas for the Gg, T_{max} was observed at 479 °C [29]. The first T_{max} observed for the Gg-cl-PAAM at 230.2 °C was caused by the elimination of –OH groups; the second T_{max} at 377.5 °C was attributed to depolymerization reactions; and the third T_{max} at 594.5 °C driven by the elimination of imide groups from the grafted polymer chains, which formed during the initial stages of the thermal degradation process. The lower mass-loss rate observed for Gg-cl-PAAM was attributed to the introduction of crosslinks in its polymeric network.

3.2. Swelling studies

The swelling capability of hydrogels in water is one of their most important properties; in particular as most industrial applications are based on and exploit their capacity for swelling. Therefore, from an application point of view, it is very important for hydrogels to possess good swelling properties. The swelling properties of the Gg-cl-PAAM hydrogel prepared in this work were studied in double-distilled water as a function of swelling time, temperature, and pH (Figure 4).

Firstly, the swelling behavior of Gg-cl-PAAM was studied over different time intervals, revealing a gradual increase in P_s as the time increased, until an equilibrium was attained at ~20 h (Figure 4(a)). After 20 h, saturation in the weight of hydrogel was observed; this result might be caused by the full occupation of the pores of Gg-cl-PAAM, which restricts the entry of additional water molecules into the polymer network [2, 29].

The effect of temperature of the swelling medium, i.e., water, on the P_s was also investigated (Figure 4(b)). Initially, the value of P_s increased as the temperature of swelling medium increased, and this trend was followed up to a temperature of 50 ºC, whereas. After this point, the value of P_s decreased with increasing temperature. The initial increase in the value of P_s stems from an increase in the elasticity of the polymer matrix with increasing temperature. In addition, increased temperature favored the formation of hydrogen bonds, which could trap additional water molecules, thus increased the value of P_s. However, at very high temperatures (i.e., above 50 °C in this work), the hydrogen bonds were broken, leading to the release of water molecules and a decreased in the value of P_s [19].

The pH responsiveness of the swelling behavior of Gg-cl-PAAM hydrogel was tested using aqueous solutions with different pH (Figure 4(c)). The Gg-cl-PAAM hydrogel exhibited a pH dependent swelling behavior, with a maximum P_s at neutral pH. This type of swelling behavior is attributed mainly to osmotic swelling pressure (π_{ion}), which can be defined using the following expression [7, 19]:

$$\pi_{ion} = RT\sum (C_i^g - C_i^s) \qquad (4)$$

where, C_i^g and C_i^s are the molar concentrations of free ions in the gel phase and aqueous medium, respectively. The percentage swelling of hydrogels is directly proportional to the value of π_{ion}.

The structure of Gg is rich in hydroxyl and carboxylic acid groups, and exhibits therefore slightly polyelectrolyte-like character [30]. The P_s of Gg-cl-PAAM depends largely on the osmotic swelling pressure generated by the free ions within the gel phase and aqueous medium. At neutral pH, the value of π_{ion} is high because the value of C_i^s is very low. By contrast, in solutions with low pH, the value of C_i^g is low as a result of significant protonation, and reduces ultimately

the value of π_{ion}. In strongly basic solutions; the value of π_{ion} is also very low as a result of the presence of free Na^{+} and ^{-}OH ions in high concentrations [6].

3.3. Separation of saline from petroleum fractions

In our previous work, we have utilized hydrogels to separate saline water from petroleum fractions [5-7]. Therefore, in the present work, the Gg-cl-PAAM with high swelling capacity and low cost synthesis was also tested for the separation of saline water from several petroleum fractions (diesel, petrol, kerosene, and petroleum ether). Prior to the separation experiments, the capacity of Gg-cl-PAAM to absorb the various petroleum fractions in isolation was examined, revealing that Gg-cl-PAAM does not absorb any of the petroleum fractions. The saline absorption capacity of the Gg-cl-PAAM hydrogel from different emulsions was found to be in the following order: petroleum ether (42.8%) > petrol (37.45%) > kerosene (24.7%) > diesel (29.8%) (Table 3). The differences observed in the absorption of saline from different emulsions were attributed to the differences in hydrocarbon chain length of the different petroleum products. The longer chains act as a barrier for incoming water molecules and ultimately manifest as reduced absorption capacity. As a consequence, the highest saline absorption was observed in the emulsion of saline and petroleum ether because petroleum ether has the smallest chain length among all the petroleum fractions examined [6].

3.4. Flocculation characteristics

The flocculation characteristics of Gg-cl-PAAM were studied at different polymer doses (10, 15, 20, and 25 mg L^{-1}) in neutral clay suspension (Figure 5(a)). Initially, as the mass of Gg-cl-PAAM was increased, the residual turbidity decreased, with a minimum value of 1512 NTU at polymer loading of 20 mg L^{-1}. However, the residual turbidity increased again as the loading of

Gg-cl-PAAM in the clay suspension was increased. This type of flocculation behavior was attributed to the bridging mechanism through which the different functionalities present on the hydrogel structure act as bridges to form complexes between different colloidal particles [9, 15]. During bridging, particles suspended in the solution interact with the binding sites or the functionalities present in the polymer, and immediately after coming into contact, they form extended polymer chains. Therefore, residual turbidity displayed an initial decrease as the polymer dose increased as a result of the increased number of functional groups available for interaction with clay particles. By contrast, at much higher polymer concentrations, the residual turbidity increases again because the colloidal particles are enveloped by the chains of the networked polymer structure, which restricts the formation of complexes and results in a decrease in the value of residual turbidity [9, 10, 15].

Previously, solution temperature was also found to have a significant effect on flocculation characteristics when biopolymer-based materials were used as flocculants [5-7]. In our previous work, we have reported that the hydrogel polymer of Gg with the co-polymer mixture of AAM and acrylonitrile showed the temperature dependent flocculation characteristics; where initially the residual turbidity decreased with increasing temperature from 30 to 40 ºC. Furthermore, with increase in temperature above 40 ºC resulted in an increased value of residual turbidity [5]. Therefore, the temperature of the clay suspension was varied in this work and the results obtained are depicted in Figure 5(b). Initially, the flocculation efficiency increased with increasing temperature and the residual turbidity reached its minimum (1376 NTU) at 40 °C. This result can be attributed to the enhanced swelling at higher temperatures, which also favors the bridging process. As the temperature increased further, the colloidal particles were re-dispersed again, leading to an increased value of residual turbidity [5-7].

Analysis of the pH dependency of the flocculation efficiency of Gg-cl-PAAM showed that it exhibits maximum flocculation efficiency in solutions with acidic pH (Figure 5(c)). The lower value of residual turbidity observed in acidic clay suspension may be caused by the protonation of different functional groups present in Gg-cl-PAAM [5-7]. The cationic functionalities present in the acidic clay suspension interact strongly with anionic clay particles, facilitating their settling down. On the other hand, under alkaline conditions, the different functional groups are not protonated and, therefore, a comparatively higher value of residual turbidity is observed.

3.5. Comparison of swelling and flocculation properties of Gg-cl-PAAM hydrogels synthesized under different reaction conditions

The swelling capacity of Gg-cl-PAAM hydrogel synthesized via the microwave-assisted method was compared with capacity of the same polymer synthesized under different reaction conditions such as in-air [19] and under pressure, i.e., using an autoclave [29]. The comparison revealed that the hydrogel fabricated using the microwave-assisted procedure exhibited the highest P_s (2117%), and the hydrogels synthesized in-air and under pressure exhibited comparatively lower values of P_s (1426% for in-air and 1350% for under pressure). Moreover, the flocculation efficiency of Gg-cl-PAAM hydrogel prepared by microwave-irradiation was better than the efficiencies of hydrogels synthesized in-air [19]. These superior swelling and flocculation characteristics observed for the hydrogel synthesized using the microwave-assisted method are attributed to the formation of short-chain polymers [26].

3.6. Adsorption of dyes

3.6.1. Effect of different adsorption parameters

Previously, biopolymer-based hydrogels have shown good efficiency as adsorbents in the removal of different pollutants from wastewater [11, 20, 22, 27]. Therefore, the ability of Gg-cl-PAAM to remove different anionic (MO and CR) and cationic dyes (RhB and BG) from aqueous solution was tested. Initially, the mass of Gg-cl-PAAM was varied in order to establish the optimum loading for each dye, and in the case of BG, the maximum adsorption efficiency (94%) was observed at 40 mg of Gg-cl-PAAM, whereas, in the case of RhB (87%), CR (32%), and MO (30%), the maximum adsorption efficiency was observed when 50 mg of the adsorbent was used (Figure 6(a)). The absorption experiments revealed that Gg-cl-PAAM displays significantly higher adsorption efficiency for cationic dyes than for anionic dyes. This observation can be attributed to the presence of abundant carboxylate and hydroxyl groups in the main structure of Gg-cl-PAAM, which permit the formation of stronger electrostatic interactions with the cationic dyes than with the anionic dyes. Among the cationic dyes, Gg-cl-PAAM showed considerably better adsorption efficiency for BG than for RhB. This preference for BG dye over RhB stems most likely from the steric hindrance caused by the 2D planar structure of RhB molecules, which restricts the attachment of the dye molecules to the adsorption sites present on Gg-cl-PAAM [21, 31].

The dependency of the adsorption efficiency of Gg-cl-PAAM on solution pH was studied by varying the pH of the dye solutions from 2.0 to 11.0 (Figure 6(b)). For the adsorption of cationic dyes, the results showed that as the solution pH increased from strongly acidic to neutral, the adsorption efficiency increased. The comparatively lower adsorption efficiency determined in solutions with lower pH was caused by the high concentration of H^+ ions, which compete for the anionic binding sites of the adsorbent. As the solution pH increases, the concentration of H^+ ions decreases, which in turn increases the number of adsorption sites that are available for binding

the adsorbate molecules, causing thus the adsorption efficiency to increase [20, 32]. In the case of anionic dyes, a different trend was observed—namely, the absorption efficiency was higher in solutions with acidic pH than in solutions with higher pH. Furthermore, in most cases the gum polysaccharides based adsorbents, the pzc was found to be less than 4.0 [20-22, 32], which means that below this pH the surface of adsorbent, i.e. Gg-cl-PAAM, was having positive charges and adsorbed negative dye molecules. The surface charge above the pzc was negative, which reduced the adsorption of anionic dyes. Therefore, in case of anionic dyes, the higher adsorption efficiency observed in strongly acidic dye solutions, which decreased with increasing solution pH.

Typically, adsorption in cases where biopolymer-based materials are used as adsorbents is mediated by electrostatic interactions. Therefore, the adsorption behavior of all the four dyes (i.e., RhB, BG, MO, and CR) was studied in salt solutions of NaCl and $CaCl_2$ separately (Figures 6(c) and (d)). These experiments showed that as the ionic strength of metal cations (Na^+ and Ca^{+2}) in the respective salt solution increased, the adsorption efficiency of Gg-cl-PAAM for the adsorption of cationic dyes i.e. RhB and BG decreased. This decrease might be caused by the increased number of competing interactions generated by the presence of metal cations (Figure 6(c)) [22]. By contrast, in the case of anionic dyes, the presence of metal cations did not affect the performance of Gg-cl-PAAM, which suggests that the adsorption operates via the electrostatic interactions mechanism (Figure 6(d)).

3.6.2. Adsorption isotherms

The adsorption isotherm studies for all four dyes taken were performed at room temperature, with the dyes in concentration range of 50–400 mg L^{-1}. The experimental data was fitted using

the non-linear forms of Langmuir and Freundlich adsorption isotherms (Figures 7(a) and (b)). The mathematical expressions for both isotherm models are reported in the literature [22, 27, 33, 34]. Based on the values of the correlation coefficient (R^2), the Langmuir model was found to provide the best fit for the adsorption of all dyes studied in this work, with maximum adsorption capacities for BG, RhB, MO, and CR of 523.62 mg g^{-1}, 421.60 mg g^{-1}, 173.69 mg g^{-1}, 179.09 mg g^{-1}, respectively (Table 4). The adsorption capacity of Gg-cl-PAAM for the removal of different anionic and cationic dyes was compared with the capacities of some other biopolymer-based adsorbents (Table 5) [35-49], revealing that Gg-cl-PAAM displays good results in terms of potential use as an adsorbent for large-scale applications.

Previously, we have prepared the graft co-polymers of Gg with different vinyl monomers such as poly(acrylic acid) (PAA), poly(methacrylic acid) (PMAA), and their combination with PAAM under different reaction conditions, and applied them to the removal of different pollutants (mostly cationic dyes) [20, 50]. Comparison of the adsorption capacity of the Gg-cl-PAAM hydrogel prepared via microwave-assisted synthesis in the present work with other previously fabricated hydrogels containing Gg revealed that Gg-cl-PAAM shows good adsorption capacity. For example, a hydrogel nanocomposite comprised of Gg-cl-P(AA-AAM)/Fe_3O_4 showed adsorption capacity of 654.87 mg g^{-1} for the removal of RhB [20]; the Gg-cl-PAA/Fe_3O_4 hydrogel nanocomposite showed adsorption capacity of 671.14 mg g^{-1} for the adsorption of methylene blue (MB) [50], while Gg-cl-P(AAM-co-MAA) hydrogels prepared using microwave-assisted synthesis showed adsorption capacities of 694.44 and 543.47 mg g^{-1} for the adsorption of MB and methyl violet (MV), respectively [51]. The higher adsorption capacities of these hydrogels when compared to that of the Gg-cl-PAAM material prepared here can be attributed to the presence of a hydrophilic monomer such as PAA in the structure of hydrogel polymer.

3.6.3. Desorption and reusability studies

The ability of an adsorbent to retain its absorption efficiency over multiple adsorption cycles without significant losses in performance is highly desirable for large-scale industrial applications. To this end, the re-usability of Gg-cl-PAAM for the adsorption and desorption of RhB was studied over five cycles (Figure 7(c)). The Gg-cl-PAAM was found to be very stable and its adsorption efficiency remained essentially unchanged over the first three adsorption–desorption cycles. In the last two cycles, however, the adsorption efficiency decreased slightly, which might be attributed to the disintegration of the polymer network and the saturation of adsorption sites. Therefore, the results of these experiments suggest that Gg-cl-PAAM is suitable for use as an adsorbent in large-scale applications in various industries.

3.6.4. Mechanism of adsorption

The most probable mechanism of binding between the RhB dye molecules and the adsorption sites of Gg-cl-PAAM is shown in Figure 8. In this mechanism, different cationic dye molecules are adsorbed onto the anionic adsorbent mostly through electrostatic interactions since Gg is an anionic biopolymer that possesses a high concentration of hydroxyl and carboxylate ions, which can interact easily with cationic dye molecules.

3.7. Biodegradation studies

The most important characteristic of gum polysaccharides is their facile degradation under certain specific environmental conditions. Graft co-polymerization of biopolymers with different vinyl monomers should ideally improves their properties while at the same time leaving their

ability to degrade unaffected. Therefore, it is important for the synthesis not have harmful effect on the environmental friendliness and biodegradability of the employed biopolymers. In the present work, the impact of grafting on the degradability of the Gg-cl-PAAM structure was tested using the soil-burial method. Once the samples were buried, samples were taken every 5 days, and their weights measured. During the initial stages of the experiment, i.e. in the starting 10 days, the rate of biodegradation of Gg-cl-PAAM was much slower, but after 10 days the rate of degradation increased progressively. This slower degradation rate in the starting 10 days was because of the hard and dry sample surface, which hindered the attack of microorganisms. However, once the surface wetness increased, it was easier for the microorganisms to accelerate the process of degradation. As a consequence, the rate of biodegradation increased over time and up to 93% of the Gg-cl-PAAM degraded within the time span of 60 days (Figure 9). Furthermore, the color of the sample changed from brown to black as the degradation process progressed. Therefore, it can be concluded that the after grafting of Gg with AAM did not diminish its environmentally friendly character and the Gg-cl-PAAM hydrogel was successfully degraded using the soil-burial method [7, 52].

3.7.1. Evidence of biodegradation

During the bio-degradation process, the samples of Gg-cl-PAAM hydrogel were examined by FTIR spectroscopy to reveal any changes in position or intensity of the peaks associated with different functional groups when compared to those of the pristine non-degraded sample (Figure 10). During the first stage of biodegradation, which involves the initiation of the degradation process, the positions of several peaks were found to change, namely, the peak originally observed at 1669 cm^{-1} shifted to 1723 cm^{-1}, the peak at 1109 cm^{-1} shifted to 1167 cm^{-1}, and the peak at 2372 cm^{-1} shifted to 2372 cm^{-1}. In addition, the intensities of the peaks at 3421 cm^{-1} and

2937 cm^{-1} decreased significantly (Figure 10(a)). The FTIR spectrum obtained during the second stage revealed the disappearance of peaks characteristic for components such as Gg and PAAM (Figure 10(b)). This stage of biodegradation is associated with the cleavage of PAAM chains from the polymer backbone, and represents the main reason for the disappearance of the peaks arising from the individual components. The FTIR spectrum collected during the last stage revealed that some of the peaks that were initially present were either completely shifted to different positions or completely absent (Figure 10(c)) as a result of the complete rapture of the polymer structure mediated by the attack of microorganisms [7].

Figure 11(a–d) shows the SEM images of the polymers before and after the degradation. Prior to degradation, the morphology of the polymer was smooth, continuous, and crack-free (Figure 11(a)). In the initial stages of the degradation, the smooth and continuous morphology started to change into rough and heterogeneous morphology. The SEM image of the sample collected during the first stage exhibited irregular and heterogeneous morphology caused by the presence of some cracks (Figure 11(b)). During the next stage of degradation, these cracks became larger in size and increased in number (Figure 11(c)). The SEM image obtained for the sample collected during the last stage revealed that the morphology of the surface was completely destroyed, indicating the complete breakdown of the hydrogel polymer (Figure 11(d)).

4. Conclusions

In the present work, Gg-cl-PAAM hydrogel was synthesized successfully via microwave-assisted grafting of Gg with AAM. The swelling properties of Gg-cl-PAAM were influenced significantly by temperature and solution pH, and the maximum P_s of 2117% was observed at neutral pH and temperature of 50 °C. Furthermore, Gg-cl-PAAM was successfully utilized in the

separation of saline from different petroleum fraction emulsions. Gg-cl-PAAM showed excellent flocculation characteristics in acidic media with polymer concentration of 20 mg L^{-1}. The adsorption of different dyes onto Gg-cl-PAAM followed the Langmuir isotherm model in each case, with BG, RhB, CR, and MO displaying absorption capacities of 523.62 mg g^{-1}, 421.60 mg g^{-1}, 179.09 mg g^{-1}, and 173.69 mg g^{-1}, respectively. The adsorption capacity of Gg-cl-PAAM for the four dyes was pH-dependent and driven by electrostatic interactions. Furthermore, a significantly better adsorption efficiency was observed for cationic dyes when compared to the anionic dyes. The Gg-cl-PAAM degraded by 93% within 60 days when tested using the soil burial biodegradation method.

Acknowledgement

The authors thank the Khalifa University of Science and Technology (HM and SMA) and the Council for Scientific and Industrial Research (SSR) for financial support.

5. References

[1] S. Hermanova, R. Balkova, S. Voberkova, I. Chamradova, J. Omelkova, L. Richtera, L. Mravcova, J. Jancar, Biodegradation study on poly(ε-caprolactone) with bimodal molecular weight distribution, Journal of Applied Polymer Science 127 (2013) 4726-4735.

[2] B.S. Kaith, R. Jindal, H. Mittal, K. Kumar, Synthesis of Crosslinked Networks of Gum ghatti with Different Vinyl Monomer Mixtures and Effect of Ionic Strength of Various Cations on its Swelling Behavior, International Journal of Polymeric Materials and Polymeric Biomaterials 61(2) (2012) 99-115.

[3] K. Kumar, B.S. Kaith, R. Jindal, H. Mittal, Gamma-radiation initiated synthesis of Psyllium and acrylic acid-based polymeric networks for selective absorption of water from

different oil–water emulsions, Journal of Applied Polymer Science 124(6) (2012) 4969-4977.

[4] E. Nazarzadeh Zare, M. Mansour Lakouraj, M. Mohseni, Biodegradable polypyrrole/dextrin conductive nanocomposite: Synthesis, characterization, antioxidant and antibacterial activity, Synthetic Metals 187 (2014) 9-16.

[5] H. Mittal, R. Jindal, B.S. Kaith, A. Maity, S.S. Ray, Synthesis and flocculation properties of gum ghatti and poly(acrylamide-co-acrylonitrile) based biodegradable hydrogels, Carbohydrate Polymers 114 (2014) 321-329.

[6] H. Mittal, R. Jindal, B.S. Kaith, A. Maity, S.S. Ray, Flocculation and adsorption properties of biodegradable gum-ghatti-grafted poly(acrylamide-co-methacrylic acid) hydrogels, Carbohydrate Polymers 115 (2015) 617-628.

[7] H. Mittal, A. Maity, S.S. Ray, Gum ghatti and poly(acrylamide-co-acrylic acid) based biodegradable hydrogel-evaluation of the flocculation and adsorption properties, Polymer Degradation and Stability 120 (2015) 42-52.

[8] B. Bolto, J. Gregory, Organic polyelectrolytes in water treatment, Water Research 41(11) (2007) 2301-2324.

[9] L. Ghimici, M. Constantin, G. Fundueanu, Novel biodegradable flocculanting agents based on pullulan, Journal of Hazardous Materials 181(1–3) (2010) 351-358.

[10] L. Ghimici, S. Morariu, M. Nichifor, Separation of clay suspension by ionic dextran derivatives, Separation and Purification Technology 68(2) (2009) 165-171.

[11] H. Mittal, S.B. Mishra, A.K. Mishra, B.S. Kaith, R. Jindal, S. Kalia, Preparation of poly(acrylamide-co-acrylic acid)-grafted gum and its flocculation and biodegradation studies, Carbohydrate Polymers 98(1) (2013) 397-404.

[12] S. Piriyaprasarth, P. Sriamornsak, Flocculating and suspending properties of commercial citrus pectin and pectin extracted from pomelo (Citrus maxima) peel, Carbohydrate Polymers 83(2) (2011) 561-568.

[13] K.K. Das, P. Somasundaran, A kinetic investigation of the flocculation of alumina with polyacrylic acid, Journal of Colloid and Interface Science 271(1) (2004) 102-109.

[14] R. Ferretti, J. Zhang, J. Buffle, Kinetics of hematite aggregation by polyacrylic acid: effect of polymer molecular weights, Colloids and Surfaces A: Physicochemical and Engineering Aspects 121(2–3) (1997) 203-215.

[15] L. Ghimici, M. Nichifor, Novel biodegradable flocculanting agents based on cationic amphiphilic polysaccharides, Bioresource Technology 101(22) (2010) 8549-8554.

[16] Y. Adachi, Dynamic aspects of coagulation and flocculation, Advances in Colloid and Interface Science 56 (1995) 1-31.

[17] A.V. Dobrynin, M. Rubinstein, Theory of polyelectrolytes in solutions and at surfaces, Progress in Polymer Science 30(11) (2005) 1049-1118.

[18] M.M. Mishra, A. Sand, D.K. Mishra, M. Yadav, K. Behari, Free radical graft copolymerization of N-vinyl-2-pyrrolidone onto k-carrageenan in aqueous media and applications, Carbohydrate Polymers 82(2) (2010) 424-431.

[19] H. Mittal, S.B. Mishra, A.K. Mishra, B.S. Kaith, R. Jindal, Flocculation characteristics and biodegradation studies of Gum ghatti based hydrogels, International Journal of Biological Macromolecules 58 (2013) 37-46.

[20] H. Mittal, S.B. Mishra, Gum ghatti and Fe3O4 magnetic nanoparticles based nanocomposites for the effective adsorption of rhodamine B, Carbohydrate Polymers 101 (2014) 1255-1264.

[21] E. Fosso-Kankeu, H. Mittal, S.B. Mishra, A.K. Mishra, Gum ghatti and acrylic acid based biodegradable hydrogels for the effective adsorption of cationic dyes, Journal of Industrial and Engineering Chemistry 22 (2015) 171-178.

[22] H. Mittal, A. Maity, S.S. Ray, Synthesis of co-polymer-grafted gum karaya and silica hybrid organic–inorganic hydrogel nanocomposite for the highly effective removal of methylene blue, Chemical Engineering Journal 279(0) (2015) 166-179.

[23] M. Yadav, A. Sand, M.M. Mishra, J. Tripathy, V.S. Pandey, K. Behari, Synthesis, characterization and applications of graft copolymer (κ-carrageenan-g-vinylsulfonic acid), International Journal of Biological Macromolecules 50(3) (2012) 826-832.

[24] M. Yadav, D.K. Mishra, A. Sand, K. Behari, Modification of alginate through the grafting of 2-acrylamidoglycolic acid and study of physicochemical properties in terms of swelling capacity, metal ion sorption, flocculation and biodegradability, Carbohydrate Polymers 84(1) (2011) 83-89.

[25] V. Singh, P. Kumar, R. Sanghi, Use of microwave irradiation in the grafting modification of the polysaccharides – A review, Progress in Polymer Science 37(2) (2012) 340-364.

[26] H. Mittal, B.S. Kaith, R. Jindal, S.B. Mishra, A.K. Mishra, A comparative study on the effect of different reaction conditions on graft co-polymerization, swelling, and thermal properties of Gum ghatti-based hydrogels, Journal of Thermal Analysis and Calorimetry 119(1) (2014) 131-144.

[27] H. Mittal, A. Maity, S. Sinha Ray, The Adsorption of Pb2+ and Cu2+ onto Gum Ghatti-Grafted Poly(acrylamide-co-acrylonitrile) Biodegradable Hydrogel: Isotherms and Kinetic Models, The Journal of Physical Chemistry B 119(5) (2015) 2026-2039.

[28] A. Jha, S. Agarwal, A. Mishra, J.S.P. Rai, Synthesis, characterization and flocculation efficiency of poly(acrylamide-co-acrylic acid) in tanne, Iranian Polymer Journal 10 (2001) 85-90.

[29] B.S. Kaith, R. Jindal, H. Mittal, K. Kumar, Synthesis, characterization and swelling behavior evaluation of gum ghatti and acrylamide based hydro-gel for selective absorption of saline from different petroleum fraction—saline emulsions, Journal of Applied Polymer Science 124 (2012) 2037-2047.

[30] J. Kang, Q. Guo, G.O. Phillips, S.W. Cui, Understanding the structure–emulsification relationship of gum ghatti – A review of recent advances, Food Hydrocolloids 42, Part 1 (2014) 187-195.

[31] H. Ma, J.-B. Li, W.-W. Liu, M. Miao, B.-J. Cheng, S.-W. Zhu, Novel synthesis of a versatile magnetic adsorbent derived from corncob for dye removal, Bioresource Technology 190 (2015) 13-20.

[32] H. Mittal, V. Parashar, S.B. Mishra, A.K. Mishra, Fe3O4 MNPs and gum xanthan based hydrogels nanocomposites for the efficient capture of malachite green from aqueous solution, Chemical Engineering Journal 255(0) (2014) 471-482.

[33] A.R. Bagheri, M. Ghaedi, A. Asfaram, R. Jannesar, A. Goudarzi, Design and construction of nanoscale material for ultrasonic assisted adsorption of dyes: Application of derivative spectrophotometry and experimental design methodology, Ultrasonics Sonochemistry 35 (2017) 112-123.

[34] H.Z. Khafri, M. Ghaedi, A. Asfaram, M. Safarpoor, Synthesis and characterization of ZnS:Ni-NPs loaded on AC derived from apple tree wood and their applicability for

the ultrasound assisted comparative adsorption of cationic dyes based on the experimental design, Ultrasonics Sonochemistry 38 (2017) 371-380.

[35] S. Arellano-Cárdenas, S. López-Cortez, M. Cornejo-Mazón, J.C. Mares-Gutiérrez, Study of malachite green adsorption by organically modified clay using a batch method, Applied Surface Science 280 (2013) 74-78.

[36] C.A. Başar, Applicability of the various adsorption models of three dyes adsorption onto activated carbon prepared waste apricot, Journal of Hazardous Materials 135(1) (2006) 232-241.

[37] A. Asfaram, M. Ghaedi, M.H. Ahmadi Azqhandi, A. Goudarzi, S. Hajati, Ultrasound-assisted binary adsorption of dyes onto Mn@ CuS/ZnS-NC-AC as a novel adsorbent: Application of chemometrics for optimization and modeling, Journal of Industrial and Engineering Chemistry 54 (2017) 377-388.

[38] G.H. Sonawane, V.S. Shrivastava, Kinetics of decolourization of malachite green from aqueous medium by maize cob (Zea maize): An agricultural solid waste, Desalination 247(1) (2009) 430-441.

[39] A.R. Bagheri, M. Ghaedi, A. Asfaram, S. Hajati, A.M. Ghaedi, A. Bazrafshan, M.R. Rahimi, Modeling and optimization of simultaneous removal of ternary dyes onto copper sulfide nanoparticles loaded on activated carbon using second-derivative spectrophotometry, Journal of the Taiwan Institute of Chemical Engineers 65 (2016) 212-224.

[40] H.M.H. Gad, A.A. El-Sayed, Activated carbon from agricultural by-products for the removal of Rhodamine-B from aqueous solution, Journal of Hazardous Materials 168(2) (2009) 1070-1081.

[41] G.C. Panda, S.K. Das, A.K. Guha, Jute stick powder as a potential biomass for the removal of congo red and rhodamine B from their aqueous solution, Journal of Hazardous Materials 164(1) (2009) 374-379.

[42] H. Lata, V.K. Garg, R.K. Gupta, Adsorptive removal of basic dye by chemically activated Parthenium biomass: equilibrium and kinetic modeling, Desalination 219(1) (2008) 250-261.

[43] H. Mittal, A. Maity, S.S. Ray, Gum karaya based hydrogel nanocomposites for the effective removal of cationic dyes from aqueous solutions, Applied Surface Science 364 (2016) 917-930.

[44] H.Y. Zhu, R. Jiang, Y.Q. Fu, J.H. Jiang, L. Xiao, G.M. Zeng, Preparation, characterization and dye adsorption properties of γ-Fe2O3/SiO2/chitosan composite, Applied Surface Science 258(4) (2011) 1337-1344.

[45] R. Huang, Q. Liu, J. Huo, B. Yang, Adsorption of methyl orange onto protonated cross-linked chitosan, Arabian Journal of Chemistry 10(1) (2017) 24-32.

[46] S. Chen, J. Zhang, C. Zhang, Q. Yue, Y. Li, C. Li, Equilibrium and kinetic studies of methyl orange and methyl violet adsorption on activated carbon derived from Phragmites australis, Desalination 252(1) (2010) 149-156.

[47] V.S. Munagapati, D.-S. Kim, Adsorption of anionic azo dye Congo Red from aqueous solution by Cationic Modified Orange Peel Powder, Journal of Molecular Liquids 220 (2016) 540-548.

[48] X. Tian, C. Li, H. Yang, Z. Ye, H. Xu, Spent mushroom: a new low-cost adsorbent for removal of Congo Red from aqueous solutions, Desalination and Water Treatment 27(1-3) (2011) 319-326.

[49] S. Chatterjee, S. Chatterjee, B.P. Chatterjee, A.K. Guha, Adsorptive removal of congo red, a carcinogenic textile dye by chitosan hydrobeads: Binding mechanism, equilibrium and kinetics, Colloids and Surfaces A: Physicochemical and Engineering Aspects 299(1) (2007) 146-152.

[50] H. Mittal, N. Ballav, S.B. Mishra, Gum ghatti and Fe3O4 magnetic nanoparticles based nanocomposites for the effective adsorption of methylene blue from aqueous solution, Journal of Industrial and Engineering Chemistry 20(4) (2014) 2184-2192.

[51] H. Mittal, A. Maity, S.S. Ray, Effective removal of cationic dyes from aqueous solution using gum ghatti-based biodegradable hydrogel, International Journal of Biological Macromolecules 79 (2015) 8-20.

[52] M. Maiti, B.S. Kaith, R. Jindal, A.K. Jana, Synthesis and characterization of corn starch based green composites reinforced with Saccharum spontaneum L graft copolymers prepared under micro-wave and their effect on thermal, physio-chemical and mechanical properties, Polymer Degradation and Stability 95(9) (2010) 1694-1703.

Captions to the figures and tables

Table 1. Optimization of different grafting parameters for the synthesis of Gg-cl-PAAM

Table 2. Comparison of percentage thermal decompositions of Gg and Gg-cl-PAAM hydrogel polymer (IDT = Initial decomposition temperature and FDT = Final decomposition temperature)

Table 3. Percentage removal of saline from different petroleum fraction–saline emulsions

Table 4. The fitted parameters and corresponding error values determined for the individual adsorption isotherm models (polymer dose = 40 mg for BG, 50 mg for RhB, MO, and CR; dye solution volume = 50 mL, dye concentration = 50–400 mg L^{-1})

Table 5. Comparison of the adsorption capacity of Gg-cl-PAAM synthesized using microwave-assisted grafting for the removal of different dyes with those of other reported adsorbents

Figure 1. Proposed mechanism of microwave-assisted graft co-polymerization of AAM onto Gg.

Figure 2. FTIR spectrum of the Gg-cl-PAAM.

Figure 3. (a) TGA and **(b)** DTG thermograms of Gg-cl-PAAM.

Figures 4. The effect of **(a)** swelling time (at room temperature and neutral solution pH); **(b)** temperature (swelling time = 20 h and solution pH = 7.0) and **(c)** solution pH (swelling time 20 h and solution temperature = 50 ^{o}C) on P_s.

Figures 5. The effect of **(a)** polymer dose (at room temperature and neutral pH); **(b)** temperature (polymer dose = 20 mg L^{-1} and solution pH = 7.0) and **(c)** solution pH

(polymer dose = 20 mg L^{-1} and solution temperature = 40 ºC) on the flocculation efficiency of Gg-cl-PAAM hydrogel polymer.

Figure 6. The effect of (a) polymer dose (solution pH = 7.0, dye solution volume = 50 mL); (b) dye solution pH (polymer dose = 40 mg for BG, 50 mg for RhB, CR, and MO, solution volume = 50 mL); (c) ionic strength of cations, i.e., Na^{+} and Ca^{2+} (polymer dose = 40 mg for BG, 50 mg for RhB, solution volume = 50 mL) in solution of cationic dyes and (d) ionic strength of cations, i.e., Na^{+} and Ca^{2+} (polymer dose = 50 mg for CR and MO, solution volume = 50 mL) in solution of anionic dyes on the adsorption efficiency of Gg-cl-PAAM toward cationic and anionic dyes.

Figure 7. Non-linear fitted curves of the Langmuir and Freundlich isotherms obtained for (a) cationic dyes (polymer dose = 40 mg for BG and 50 mg for RhB, solution pH = 7.0 solution volume = 50 mL, and dye concentration = 50–400 mg L^{-1}); (b) anionic dyes (polymer dose = 50 mg, solution pH = 2.0 solution volume = 50 mL, and dye concentration = 50–400 mg L^{-1}), and (c) plot for the adsorption–desorption of RhB dye.

Figure 8. Suggested mechanism for the adsorption of RhB dye molecules onto the binding sites on Gg-cl-PAAM.

Figure 9. The progress of degradation of Gg-cl-PAAM hydrogel polymer as a function of time.

Figure 10. FTIR spectra of the Gg-cl-PAAM hydrogel polymer obtained during (a) stage-I of biodegradation; (b) stage-II of biodegradation, and (c) stage-III of biodegradation.

Figures 11. SEM images of Gg-cl-PAAM hydrogel polymer (a) prior to degradation, and during (b) stage-I of biodegradation; (c) stage-II of biodegradation, and (d) stage-III of biodegradation.

Table 1. Optimization of different grafting parameters for the synthesis of Gg-cl-PAAM

Sample	Reaction time / s	Double distilled water / mL	Initiator ratio / ABC:KPS	[AAM] (mol L^{-1})	[oMBA] (mL L^{-1})	% GY	% PL	% GE	P_s
Gg-cl-PAAM-1	30	10	1:1	0.7042	0.0649	21	31.96	154.8	765
Gg-cl-PAAM-2	60	10	1:1	0.7042	0.0649	45	55.39	123.61	927
Gg-cl-PAAM-3	90	10	1:1	0.7042	0.0649	65	76.46	117.90	1095
Gg-cl-PAAM-4	120	10	1:1	0.7042	0.0649	51	65.32	128.64	954
Gg-cl-PAAM-5	150	10	1:1	0.7042	0.0649	39	43.19	111.02	848
Gg-cl-PAAM-6	180	10	1:1	0.7042	0.0649	23	45.95	204.31	724
Gg-cl-PAAM-7	90	5	1:1	0.7042	0.0649	31	32.47	104.9	713
Gg-cl-PAAM-8	90	7.5	1:1	0.7042	0.0649	49	52.28	106.83	928
Gg-cl-PAAM-9	90	10	1:1	0.7042	0.0649	65	76.46	117.90	1095
Gg-cl-PAAM-10	90	12.5	1:1	0.7042	0.0649	43	49.67	115.88	904
Gg-cl-PAAM-11	90	15	1:1	0.7042	0.0649	28	32.31	115.96	787
Gg-cl-PAAM-12	90	10	0.25:1	0.7042	0.0649	21	23.43	112.15	1247
Gg-cl-PAAM-13	90	10	0.5:1	0.7042	0.0649	78	81.53	104.58	1465
Gg-cl-PAAM-14	90	10	0.75:1	0.7042	0.0649	71	79.46	112.08	1211
Gg-cl-PAAM-15	90	10	1:1	0.7042	0.0649	65	57.46	88.218	1095
Gg-cl-PAAM-16	90	10	1.25:1	0.7042	0.0649	34	35.68	105.09	956
Gg-cl-PAAM-17	90	10	0.5:1	0.563	0.0649	70.22	72.26	102.94	726
Gg-cl-PAAM-18	90	10	0.5:1	0.633	0.0649	71.75	73.23	102.09	1085
Gg-cl-PAAM-19	90	10	0.5:1	0.7042	0.0649	74.07	77.6	104.83	1465
Gg-cl-PAAM-20	90	10	0.5:1	0.7746	0.0649	82.65	84.61	102.40	1677
Gg-cl-PAAM-21	90	10	0.5:1	0.9859	0.0649	80.65	85.41	105.97	1858
Gg-cl-PAAM-22	90	10	0.5:1	1.056	0.0649	91.37	98.83	108.25	1769
Gg-cl-PAAM-23	90	10	0.5:1	0.9859	0.0487	86.76	95.41	110.08	1625
Gg-cl-PAAM-24	90	10	0.5:1	0.9859	0.0649	80.65	85.41	105.97	1858
Gg-cl-PAAM-25	90	10	0.5:1	0.9859	0.081	100.17	109.17	109.07	2015
Gg-cl-PAAM-26	90	10	0.5:1	0.9859	0.0974	104.71	114.25	109.19	2110
Gg-cl-PAAM-27	90	10	0.5:1	0.9859	0.01136	104.38	111.28	106.67	2062
Gg-cl-PAAM-28	90	10	0.5:1	0.9859	0.1298	126.81	135.68	107.05	1844

Where, % GY = percentage graft yield; %PL = percentage polymer loading; %GE = percentage graft efficiency and P_s = percentage swelling

Table 2. Comparison of percentage thermal decompositions of Gg and Gg-cl-PAAM hydrogel polymer (IDT = Initial decomposition temperature and FDT = Final decomposition temperature)

Sample Code	Percentage decomposition at different temperatures (K)									
	IDT	**20%**	**30%**	**40%**	**50%**	**60%**	**70%**	**80%**	**90%**	**FDT**
Gg	273.15	233.67	255.45	277.34	296.83	318.05	394.32	483.44	490.09	521.6
Gg-cl-PAAM	149.3	222.72	270.81	336.35	385.79	449.48	547.06	588.82	602.06	615.7

Table 3. Percentage removal of saline from different petroleum fraction–saline emulsions

Sample	**Percentage saline removal**[a]											
	Kerosene–saline			**Diesel–saline**			**Petrol–saline**			**Pet. ether–saline**		
	% removal	**±SD**	**±SE**	**% removal**	**±SD**	**±SE**	**% removal**	**±SD**	**±SE**	**% removal**	**±SD**	**±SE**
Gg-cl-PAAM	29.8	0.98	0.69	24.7	0.56	0.32	37.45	0.52	0.30	42.8	0.75	0.45

[a]Number of replications = 03; amount of each emulsion taken = 100 mL (1:1, v/v); weight of superabsorbent taken for each emulsion = 1.0 g

Table 4. The fitted parameters and corresponding error values determined for the individual adsorption isotherm models (polymer dose = 40 mg for BG, 50 mg for RhB, MO, and CR; dye solution volume = 50 mL, and dye concentration = 50–400 mg L^{-1})

Isotherm model	**Parameter**	**Dye**			
		RhB	**BG**	**MO**	**CR**
Langmuir	q_m (mg g^{-1})	421.60	523.62	173.69	179.09
	K_L (L mg^{-1})	0.134	0.148	0.018	0.018
	Reduced χ^2	10.86	53.63	0.827	1.059
	RSS	65.20	321.81	4.96	6.355
	R^2	0.999	0.997	0.999	0.999
Freundlich	K_F (L $mg^{-1})^{1/n}$(mg g^{-1})	176.47	148.87	24.46	25.44
	1/n	0.2164	0.199	0.319	0.318
	Reduced χ^2	2649.97	1591.96	64.988	66.59
	RSS	15899.84	9551.81	389.93	399.54
	R^2	0.870	0.856	0.935	0.938

Table 5. Comparison of the adsorption capacity of Gg-cl-PAAM synthesized using microwave-assisted grafting for the removal of different dyes with those of other reported adsorbents

Adsorbent	**Dye**	**q_m (mg g^{-1})**	**Reference**
Organoclay	BG	40.48	[35]
Waste apricot	BG	116.27	[36]
Mn@CuS/ZnS-NC-AC	BG	115.1	[37]
Maize cob powder	BG	37.037	[38]
CuS-NP-AC	BG	263.2	[39]
Gg-cl-PAAM*	BG	523.62	This study
Bagasse pitch	RhB	263.85	[40]
Jute stick powder	RhB	87.7	[41]
Modified parthenium biomass	RhB	18.5	[42]
GK-cl-PAA/SiC hydrogel nanocomposite	RhB	497.51	[43]
Gg-cl-PAAM*	RhB	421.60	This study
Y-Fe_2O_3/SiO_2/chitosan composite	MO	34.29	[44]
Protonated cross-linked chitosan	MO	89.30	[45]
Activated carbon derived from *Phragmites australis*	MO	238.1	[46]
Gg-cl-PAAM*	MO	173.69	This study
Orange peel	CR	163	[47]
Spent mushroom	CR	147.1	[48]
Chitosan beads	CR	93.7	[49]
Gg-cl-PAAM*	CR	179.09	This study

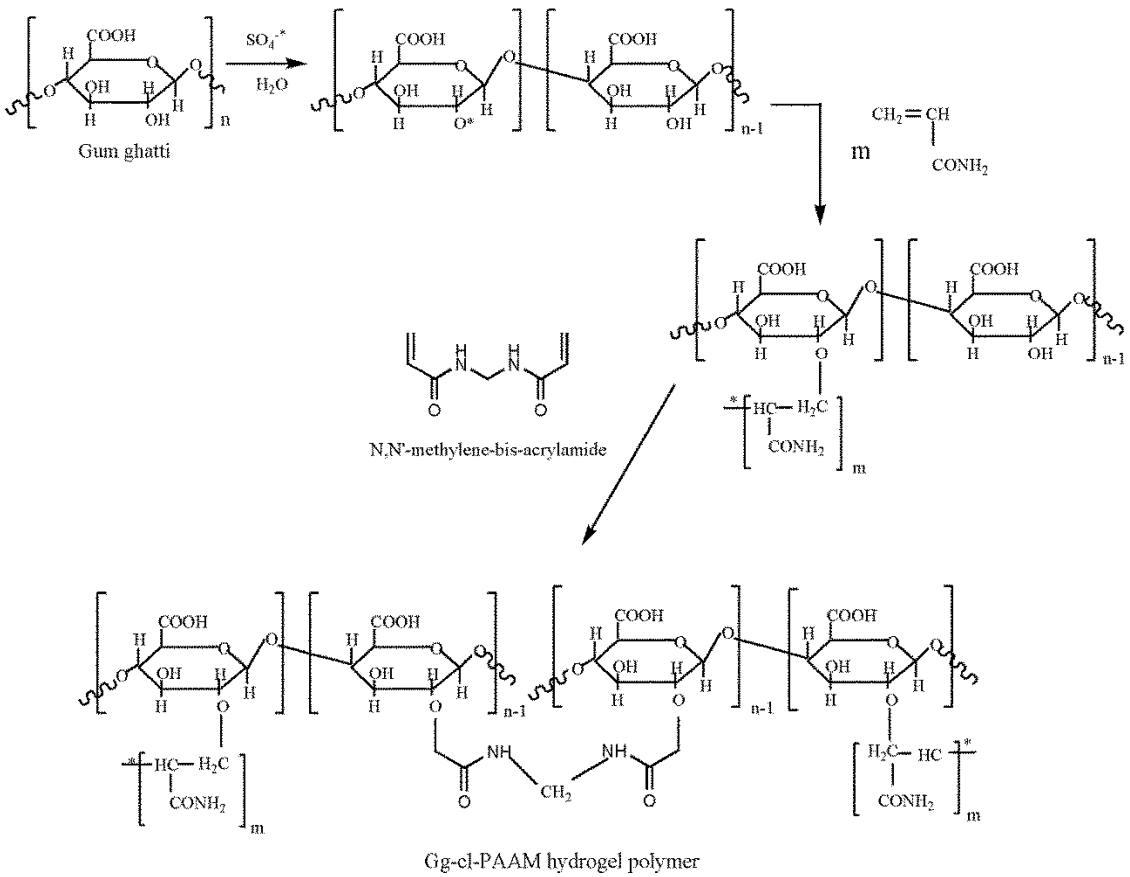
Gum ghatti
N,N'-methylene-bis-acrylamide
Gg-cl-PAAM hydrogel polymer

Figure 1

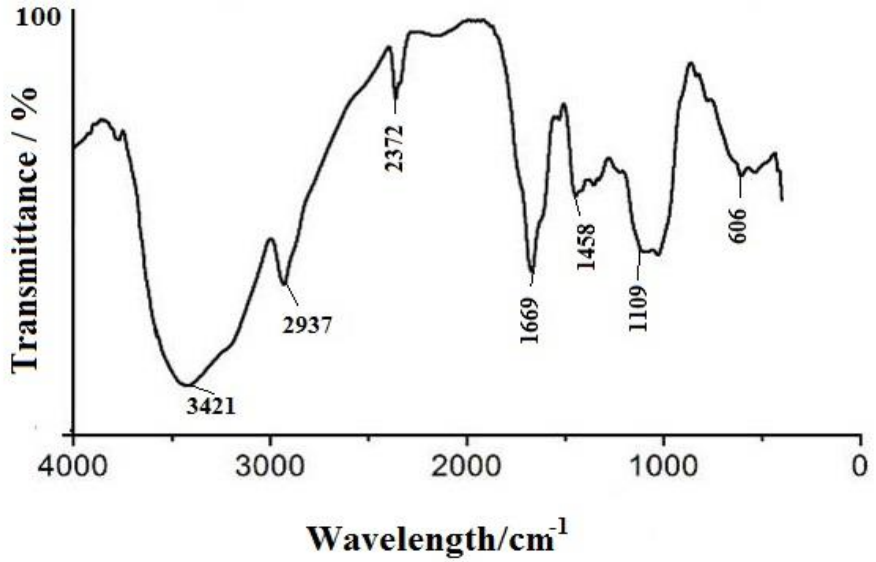
100
Transmittance / %
3421
2937
2372
1669
1458
1109
606
4000
3000
2000
1000
0
Wavelength/cm-1

Figure 2

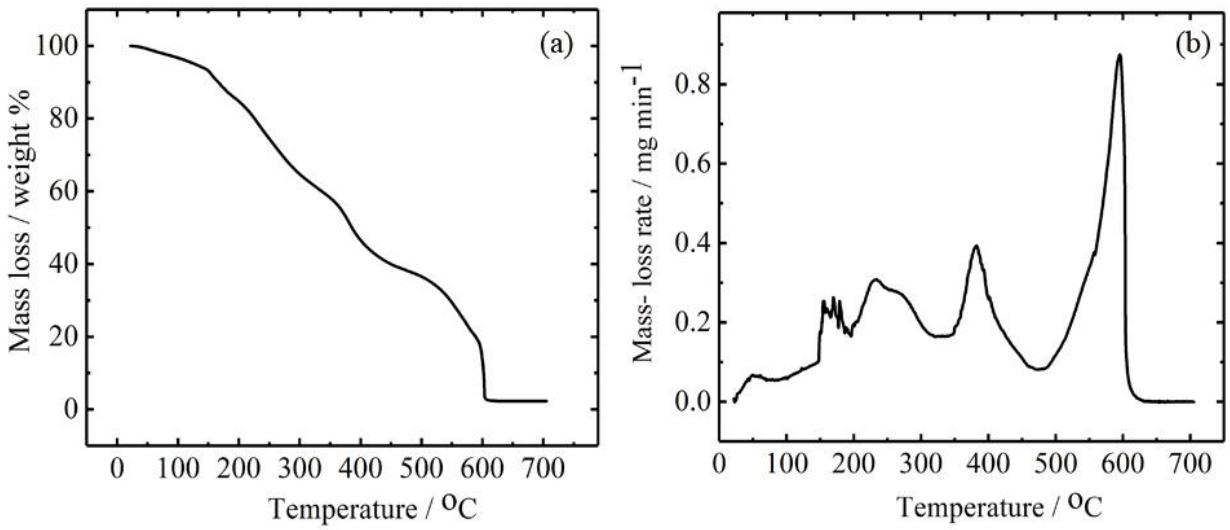
(a)
Mass loss / weight %
100
80
60
40
20
0
0 100 200 300 400 500 600 700
Temperature / °C
(b)
Mass- loss rate / mg min-1
0.8
0.6
0.4
0.2
0.0
0 100 200 300 400 500 600 700
Temperature / °C

Figure 3

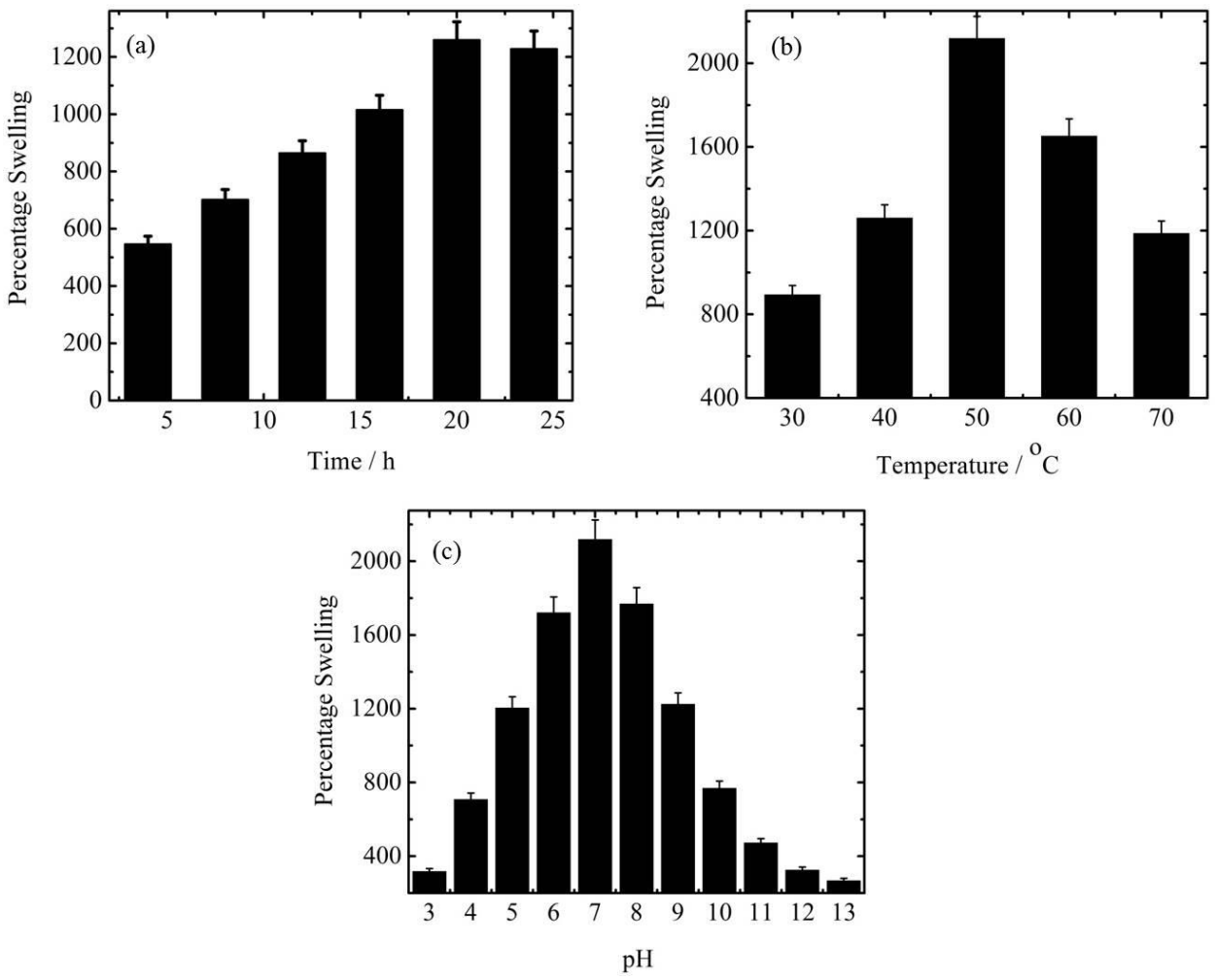
(a)
Percentage Swelling
0
200
400
600
800
1000
1200
5
10
15
20
25
Time / h
(b)
Percentage Swelling
400
800
1200
1600
2000
30
40
50
60
70
Temperature / °C
(c)
Percentage Swelling
400
800
1200
1600
2000
3
4
5
6
7
8
9
10
11
12
13
pH

Figure 4

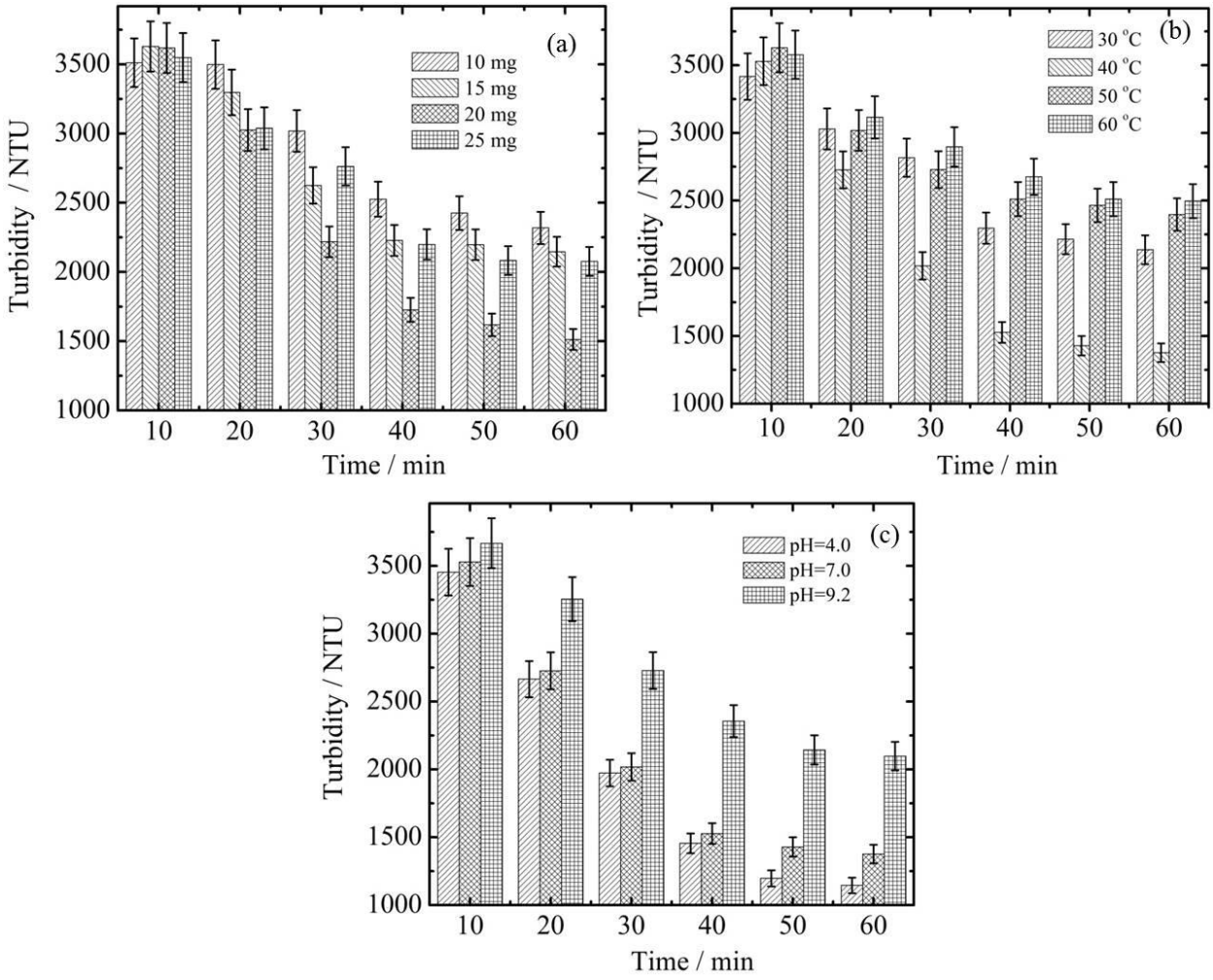
(a)
10 mg
15 mg
20 mg
25 mg
Turbidity / NTU
Time / min
(b)
30 °C
40 °C
50 °C
60 °C
Turbidity / NTU
Time / min
(c)
pH=4.0
pH=7.0
pH=9.2
Turbidity / NTU
Time / min

Figure 5

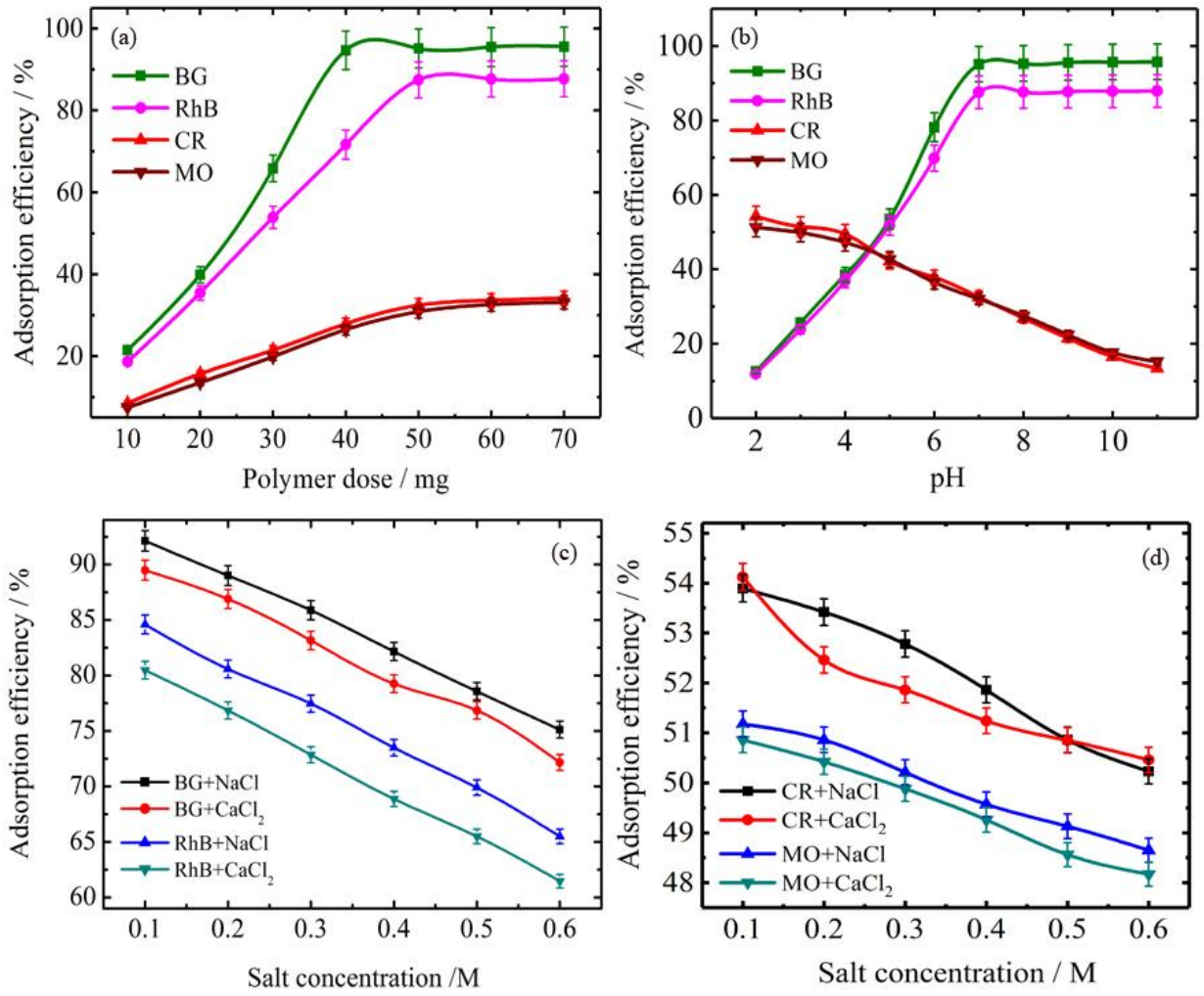
(a)
BG
RhB
CR
MO
Adsorption efficiency / %
Polymer dose / mg
(b)
pH
(c)
BG+NaCl
BG+CaCl2
RhB+NaCl
RhB+CaCl2
Salt concentration /M
(d)
CR+NaCl
CR+CaCl2
MO+NaCl
MO+CaCl2
Salt concentration / M

Figure 6

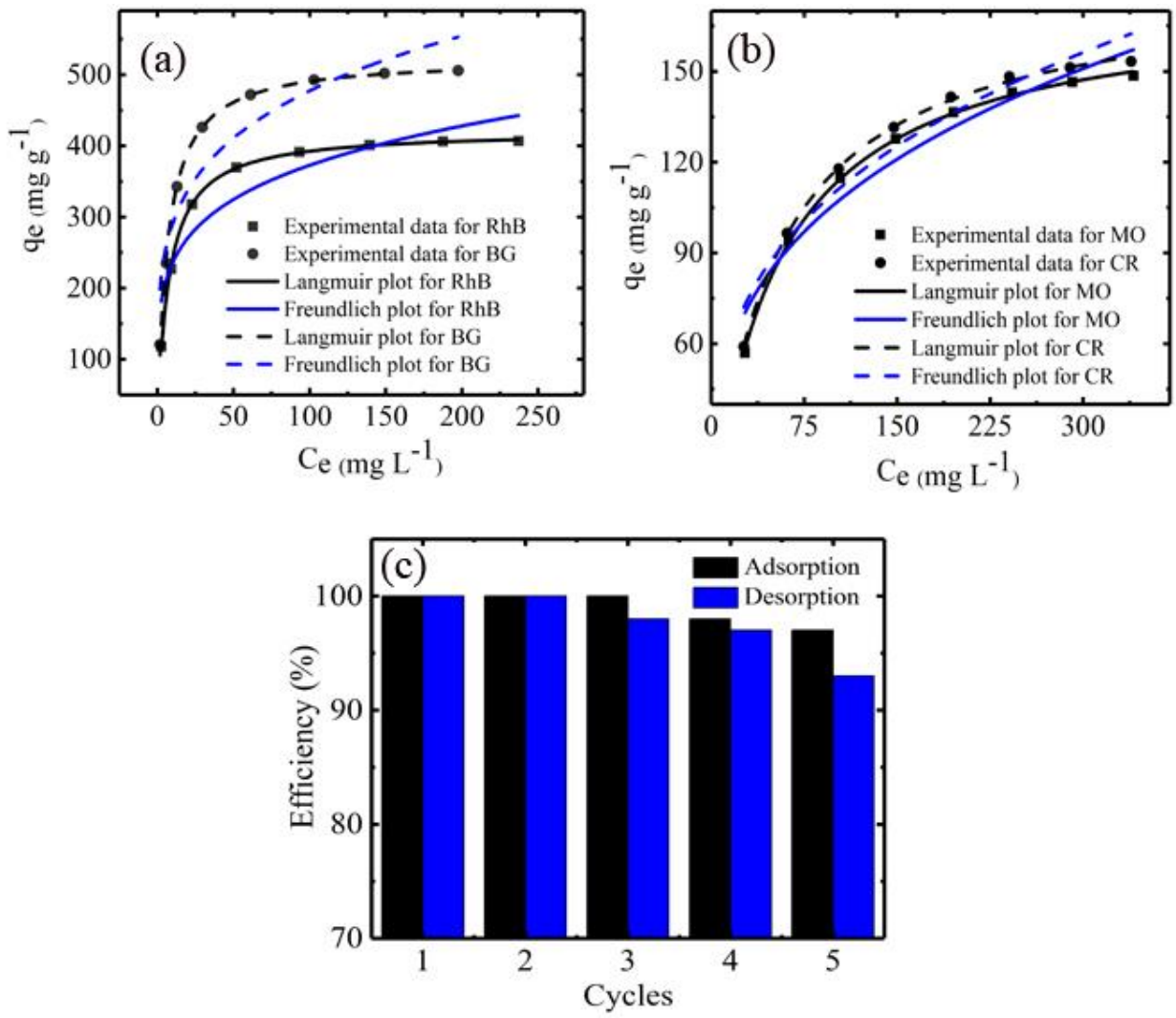
(a)
qe (mg g-1)
Ce (mg L-1)
Experimental data for RhB
Experimental data for BG
Langmuir plot for RhB
Freundlich plot for RhB
Langmuir plot for BG
Freundlich plot for BG
(b)
qe (mg g-1)
Ce (mg L-1)
Experimental data for MO
Experimental data for CR
Langmuir plot for MO
Freundlich plot for MO
Langmuir plot for CR
Freundlich plot for CR
(c)
Adsorption
Desorption
Efficiency (%)
Cycles

Figure 7

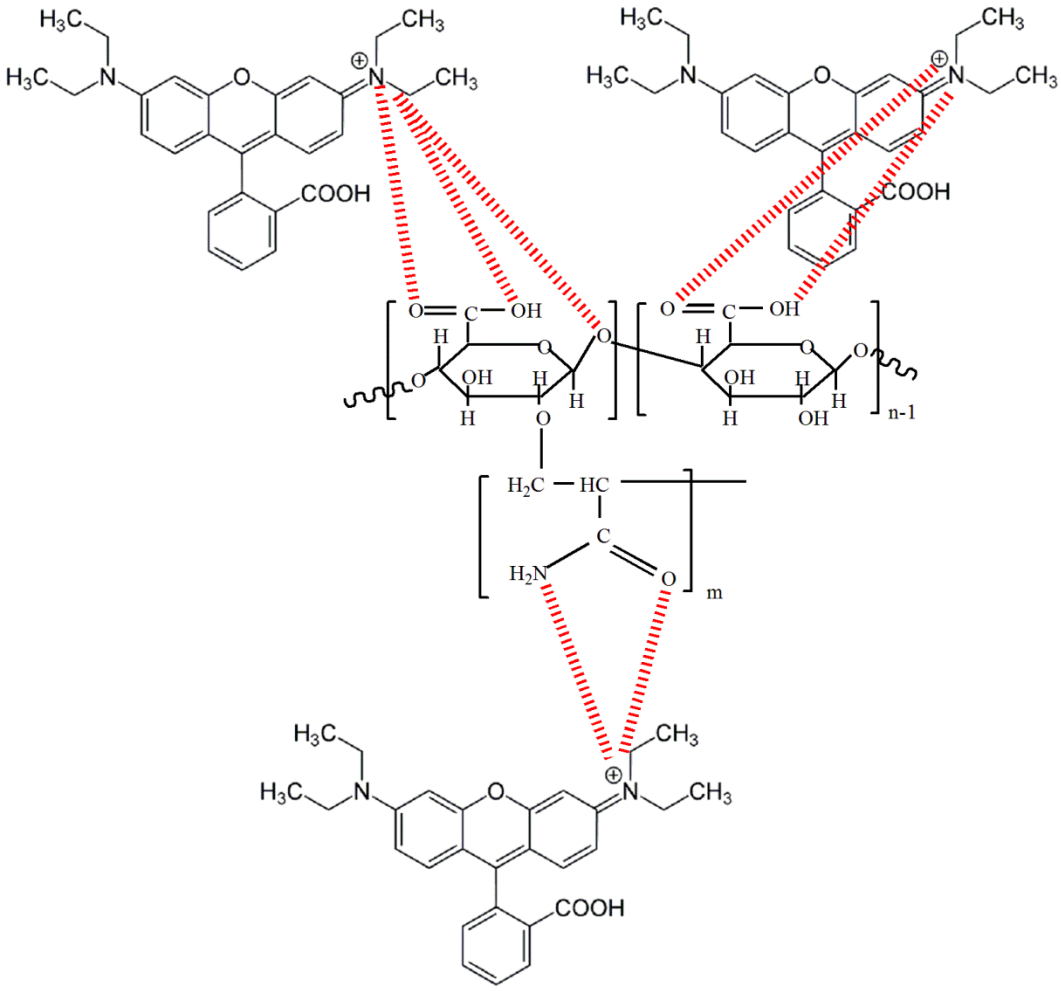

Figure 8

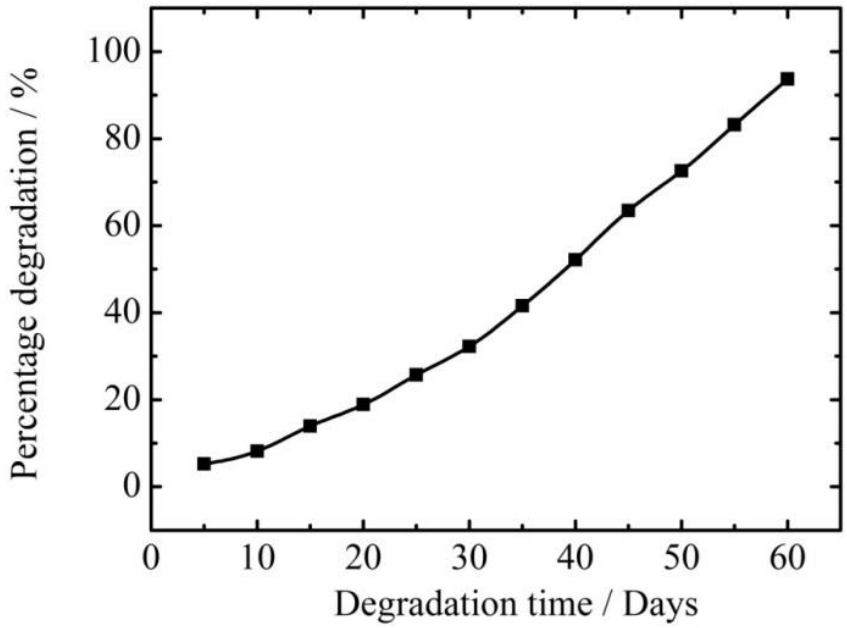
Percentage degradation / %
100
80
60
40
20
0
0
10
20
30
40
50
60
Degradation time / Days

Figure 9

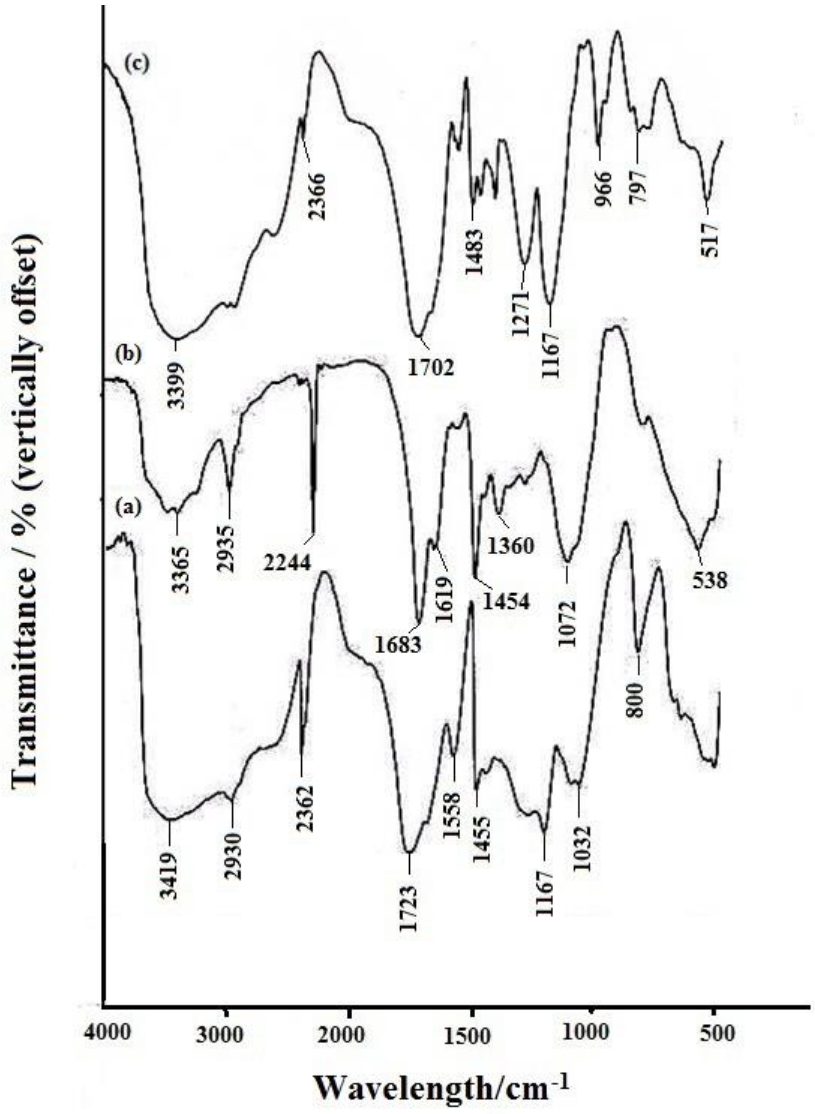
(c)
(b)
(a)
Transmittance / % (vertically offset)
3399
2366
1702
1483
1271
1167
966
797
517
3365
2935
2244
1683
1619
1454
1360
1072
538
3419
2930
2362
1723
1558
1455
1167
1032
800
4000
3000
2000
1500
1000
500
Wavelength/cm-1

Figure 10

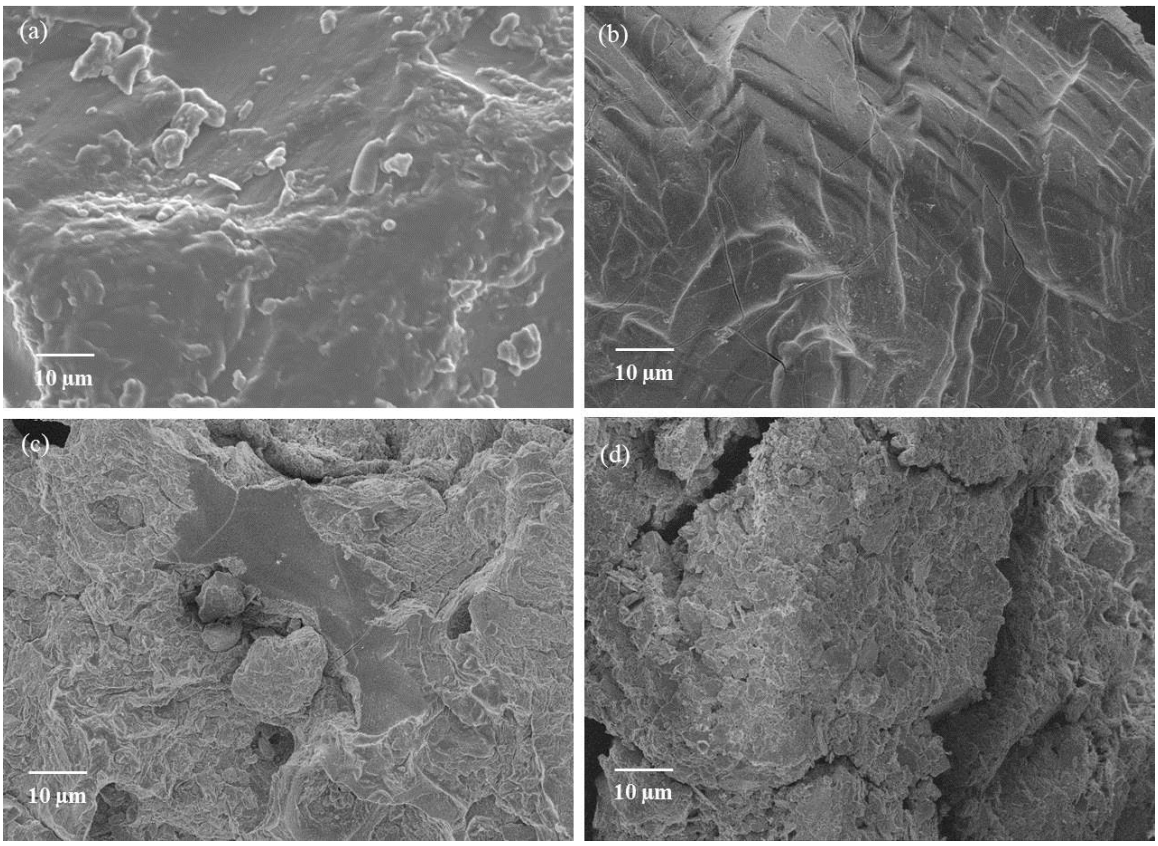

Figure 11